JOURNAL OF MATERIALS SCIENCE 35 (2000) 3467–3478

Braided composites for energy absorption under tensile loading

B. N. COX, J. B. DAVIS
Rockwell Science Center, 1049 Camino Dos Rios, Thousand Oaks, CA 91360, USA
E-mail: bncox@rsc.rockwell.com

A new class of braided composites has been designed to maximise the total energy absorbed during tensile failure. Braided loops of light, continuous fiber tows are configured in such a way that they must be drawn through relatively large displacements before they come into direct contact with one another. Upon loop contact, the material hardens locally, forcing further damage to develop by the same process elsewhere. In this way the entire gauge section absorbs energy before ultimate failure. Levels of energy absorption per unit volume reach 30 MJ/m^3 and, per unit mass, 18 J/g. The mechanisms involved in damage delocalisation and failure are detailed and modeled at a very simple level. While the current values of energy absorption are already attractive, the simple models indicate much higher values for composites that have been optimised.

1. Introduction

Many energy absorption problems involve loads that are tensile, for example, casings designed to contain bursting rotors, turbines, or flywheels; backing plates in armour systems; and containers subject to internal explosions. Here a new class of textile composites is introduced with unusually high energy absorption capacity under tensile loading.

The new composites incorporate mechanisms for ensuring that damage is broadly distributed throughout the body of a specimen or structure before the instability associated with ultimate failure sets in. Damage delocalization is promoted by incorporating a so-called lock-up mechanism, in which components of the reinforcement are arrested by physical contact with one another after displacing through the matrix. The extent of the displacement allowed before the lock-up of two elements of the reinforcement determines the global strain up to which damage can be delocalized, denoted ε_c. The total energy absorbed per unit volume is bounded from below by the product of ε_c and the magnitude of the global stress required for reinforcement displacement, σ_d. Both σ_d and ε_c can be varied over quite wide ranges by selecting materials and the geometry of the reinforcement, so that composites can be designed, for example, to avoid large stresses during energy absorption; or for maximum total energy absorption without constraint on the stress level. The levels of total energy absorbed per unit volume or per unit mass by members of the new class of composites are potentially very high.

The textile composites are variants of a concept first demonstrated with composites of carbon steel chains in a polymer or other matrix [1–3]. The chains are laid up so that the links are initially in a contracted configuration (Fig. 1a). Under tensile loading, damage begins with extensive matrix cracking, which allows neighbouring chain links to slide towards one another, crushing resin trapped between them in a state of near hydrostatic compression. The displacement of links through the resin absorbs most of the energy expended en route to ultimate failure. When two links come into direct contact, they are said to lock up: the material hardens locally, resisting further local displacement and triggering the displacement of links elsewhere in the same chain. Only when all links in a chain are in direct contact with their neighbors does the chain begin to fail by plastic deformation of the links followed by rupture of the weakest among them. The stress-strain response is typified by Fig. 1b. A plateau stress is sustained out to large strains, during the phase of link displacement. When the links are all in contact (strain $\varepsilon \approx 0.5$), the stress drops as the links begin to fail. The total energy absorbed per unit volume for chain composites fabricated to date ranges up to approximately 60 MJ/m^3 and the specific energy absorption (energy absorbed per unit mass) up to approximately 13 J/g. The former figure is superior to alternative candidates for energy absorption under tension. The latter figure is also very competitive, but the high density of the steel in chains suggests that higher specific energy absorption could be achieved if analogous composites could be made with light, strong continuous fibers.

In this paper, analogues of the chain composites are demonstrated by braiding continuous fibers. Braiding creates a reinforcement geometry that is most closely analogous to the geometry of interpenetrating links in chains. Large displacement capacity and a lockup effect can also be achieved by variants of weft knitting,

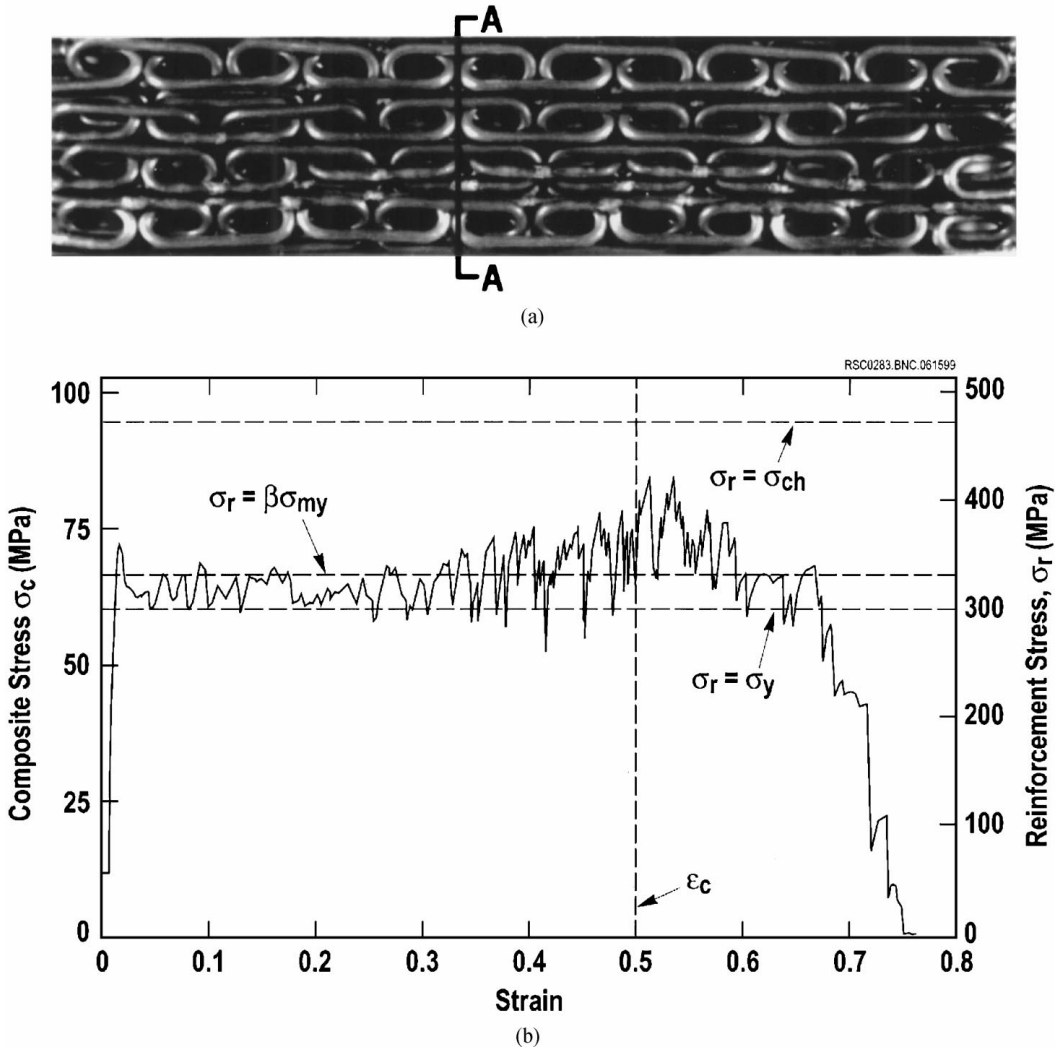

Figure 1 (a) Contracted chain configuration viewed through a transparent epoxy matrix. (b) Measured stress-strain curve for a chain/polycarbonate composite (from [3]).

but the mechanics of load transfer and lockup are different [4].

2. Fabrication of braided composites for energy absorption

The braided composites are fabricated using common continuous fibers in common matrices. The essence of the approach is to achieve the desired behavior by tailoring the reinforcement geometry, not by using exotic high-performance materials.

2.1. Braided loops

Fig. 2 illustrates the principal idea of how fiber bundles or cords can be assembled by braiding onto a set of dowel pins to simulate the contracted arrangement of links in a chain. The cords have been spread in Fig. 2 to allow their interlacing pattern to be seen more easily. In the finished composite, they are tightly packed in the horizontal direction in the figure, but retain their elongation in the vertical direction, which is the intended direction of loading.

As Fig. 2 shows, the presence of the pins allows the braided loops to interpenetrate without initially being in intimate contact. When loaded, the loops will slide and eventually make contact on the insides of their curved ends, just like the links in chain composites.

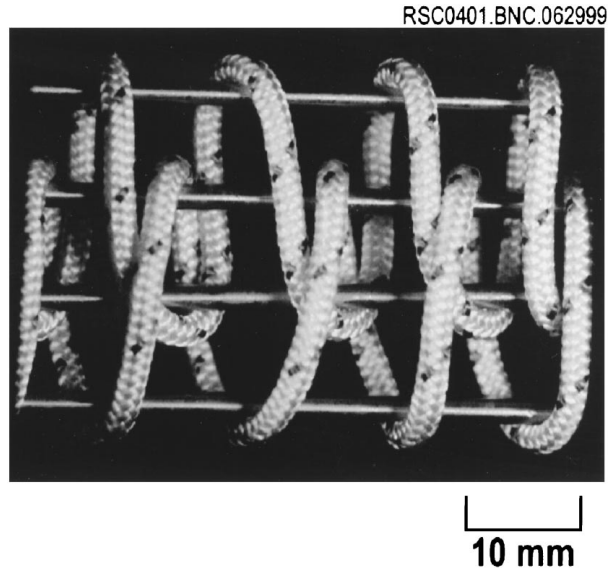

Figure 2 Cords on a set of pins with loop interlacing analogous to links of a chain.

By varying the pin spacing and the choice of pins around which the cords are looped, fabric with virtually

any sliding strain capacity and loop aspect ratio (loop length to loop width) can be fabricated.

2.2. Tooling for composite formation

After the braided fabric has been formed, it must be released from the dowel pins without relaxation of the desired geometry, infiltrated with a matrix, and consolidated. A laboratory-scale apparatus that accomplishes these tasks quite effectively is shown in Fig. 3. It consists of the array of dowel pins and their base plate (the "braiding frame" in Fig. 3) and several other components, all of which are Teflon-coated for easy release after curing of the finished composite. A plate (the "lid") containing holes slightly larger than the pin diameter is placed over the pins and against the base plate prior to braiding. The braid is then built above the lid. When the braiding is complete, the pins and fabric are inverted into a female mold (Fig. 3). Then the lid is clamped to the mold, generating sufficient compression to fix the cords in place by friction. The pins can then be withdrawn through the holes in the lid by drawing away the base plate, with minimal movement of the cords. Pistons whose heads run the length of the fabric are then pushed between the lid and the female mold by rods extending out of the mold cavity through ports, so that the fabric is further compacted by side pressure. Applying pressure in two directions assists in maximizing volume fraction. It also reduces any undesirable distortions created in the fabric when the pins are removed. Epoxy matrix is added in an uncured, inviscid state by vacuum infiltration. The epoxy is cured and the specimen is released by breaking apart the lid and female mold.

The cords to be braided are fastened initially onto the base plate, typically one at each dowel pin. The interlacing pattern is then created by passing the cords in sequence around the pins to the right and left of the pin to which they are first fastened, so that the fabric is built up continuously along a front that moves away from the base plate. During braiding, idle cords are held in tension by a system of cleats, to assist in compacting the braided fabric to an acceptably high volume fraction. It is not necessary to pass a cord end through a loop that has already been formed when producing the interpenetrating pattern. Thus one key advantage is the ease with which this process could be adapted to large scale manufacturing.

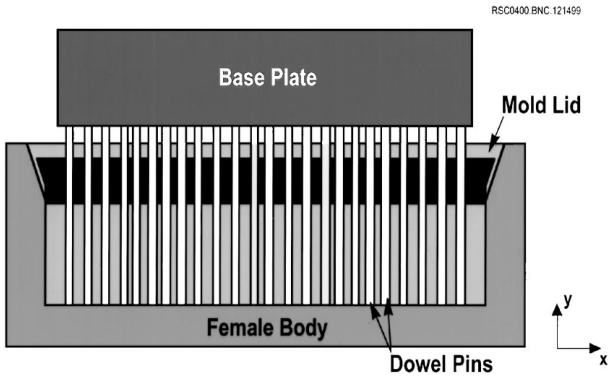

Figure 3 Apparatus for forming braided composites with high sliding strain capacity.

Because of the topology of the braiding process, loose ends of cords must remain when specimen fabrication is halted at the prescribed layer size. During loading to high strains, the loose ends tend to slide through the composite, unraveling the fabric. Unless the fabric is quite wide, the unraveling can propagate through an entire specimen. This premature failure mechanism can be averted by splicing the loose ends together to close the last row of loops. The splice must be strong enough to transmit the large loads experienced by individual cords. After considerable experimentation, the best splice that could be made by hand was found to consist simply of two cord ends laid side by side and glued together with epoxy while held fast by a wrapping of Teflon. When carefully formed, these splice joints are nearly as strong as a single straight cord.

Since the pins are coplanar, the braid built up on them will consist of a single flat layer. Laminates can be formed by stacking together layers with desired fiber orientations.

2.3. Optimal cords for braiding

The first generation of braided composites were made with loose rovings of Kevlar (or glass or carbon) fibers, which were held together relatively weakly by a small quantity of uncured polymer sizing. These tows tended to splay during braiding, especially at the crowns of loops (where tows turn around pins), which weakened them and gave them a flat, tape-like aspect. The flatness of the crowns inhibits their displacement through the matrix in the composite. As a result, failure of the reinforcement tends to precede matrix failure and reinforcement sliding, resulting in localized rather than delocalized failure; and therefore poor energy absorption characteristics.

Obtaining twisted or wrapped fiber tows that retain strength and cross-sectional aspect ratio during braiding was a major challenge. Commercial Kevlar cord was tried next, which consisted of moderately large denier tows (approximately 20k denier) sheathed in a braided skin. The commercial cord is easily handled without obvious damage and suffers a relatively small change of aspect ratio where it is bent around pins. However, the commercial cord is disappointingly loose in its packing and the majority of its fibers lie in its braided sheath, rather than in its core. The overall volume fraction of aligned Kevlar fibers achievable in the final composite is therefore low. Since the tensile strength of the cord and thus of the composite arises mainly from the aligned fibers, with the sheath contributing minimally, the ability of the cord to sustain loop displacement is severely degraded.

As an alternative to sheathed cord, a three-strand rope was fabricated by plaiting or braiding* tows of sized

* The term "braid" refers most generally to a generic textile process that involves interlacing multiple tows or yarns that are fixed at one end and fed from a system of spools or bobbins at the other. Braiding creates patterns that are topologically distinct from weaves, knits, and other textiles. In this paper, braiding usually refers to the action of

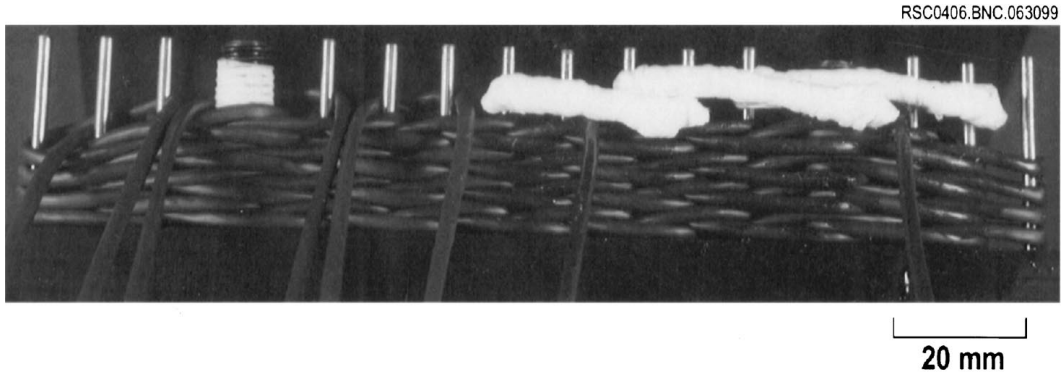

Figure 4 Braid reinforcement on nail bed showing Kevlar fiber tows (wrapped in black shrink-wrap plastic tubes to enhance fiber packing) and Teflon wrapped splices.

Kevlar together before using them for braiding. This plaited rope also exhibits reduced fiber damage and change of aspect ratio during braiding. However, because it is braided, its fibers are not aligned with the axis of the rope and therefore it cannot yield the same ultimate strength as a well compacted, sheathed cord of mainly aligned fibers.

Two solutions to the problem of forming adequate cords were eventually found. The first was to revisit the concept of sheathing axial fibers in a braided wrap. This process was done to preferred specifications using a hand-winding machine†. Large denier Kevlar tows were wrapped by a light rayon yarn wound in a fairly open pattern. Thus the ratio of axial to wrapped fibers was maintained at a high level. In spite of some variance in the skill of the operator of the hand winder, reasonably high packing densities of the aligned fibers were achieved within cords (40–50%) and the cords held together during braiding onto the dowel pins quite well.

The second solution was to encase the Kevlar tows in lengths of shrink-wrap plastic tubing. When the tubing was subsequently warmed with a hair dryer, it formed a tight sheath around the fibers. This method achieved the highest packing densities and had the further advantage of protecting the fibers during braiding. A typical braided preform made with tows in shrink-wrap tubing and partially finished with Teflon bound splices is shown in Fig. 4.

Specifications of the cords used in specimen fabrication are listed in Table I. The cord radius, r, is defined as

$$r = \sqrt{\frac{1}{\pi f \rho \psi}} \tag{1}$$

where f is the fiber packing factor in the cord, taken to be 0.7 (an indicative value only), ρ is the density of the fibers (0.00145 g/mm^3 for Kevlar), and ψ is the yield‡ of the axial fibers in the cord.

forming the composite reinforcement on the dowel pins, as illustrated in Fig. 2. However, in this section on Optimal Cords, braiding also refers to the plaiting of some tows to form thicker, more coherent cores for cords; and the wrapping of cores in a braided sheath. The reader must recognise that these are distinct steps in the processing.

† Courtesy Dr. Chris Pastore, Philadelphia College of Textiles and Science.

‡ The yield is the mass per unit length of a fiber bundle, tow, or yarn.

TABLE I Specifications of cords used

Cord label	Containment	Yield, ψ[a] (mm/g)	Cord radius, r[b] (mm)
S1[c]	None	1056	0.545
S2[d]	Shrink wrap	277	1.064
S7[e]	Wound polyester	151	1.44

[a] Yield of the core of axial fibers only.
[b] For core of axial fibers only, assuming a fiber packing factor of 0.7.
[c] Formed from a single Kevlar tow with approximately 3 weight percent resin binder.
[d] Formed from two dry Kevlar tows.
[e] Formed from seven Kevlar tows with approximately 3 weight percent resin binder.

When shrink-wrap tubing is used, resin is prevented almost entirely from entering the interior of the cord during infiltration. The only polymer present amongst the fibers of the cords during curing of the composite is the small amount of sizing on the Kevlar tows as supplied. It is not known whether the net strength of individual tows in the braided and consolidated composite is higher or lower because of this. The absence of resin may facilitate turning of the cords around nails during braiding, minimizing residual strains and physical damage in the fibers. It also changes the mechanics of load transfer between fibers in the tow as they begin to break during failure of the composite.

2.4. Geometrical characteristics of the braided composites

Fig. 5 shows schematics of two different patterns of braiding around pins, which will be called cases (a) and (b). Cord segments drawn as solid lines pass in front of the pins, while those drawn as dashed lines pass behind. The cords are drawn stretched out in the y direction for easier visualization of their interlacing. The braid pattern is periodic, with convenient unit cells as indicated by dotted lines in Fig. 5. In case (b) (Fig. 5b), pins are provided in pairs, with the left pin in each pair used exclusively for reversals of the direction of a cord to the left, and the right pin for reversals to the right. This allows abutting crowns of loops (e.g., marked C_1 and C_2 in the figure) to slide down opposite one another when the fabric is beaten up (compacted) in the y

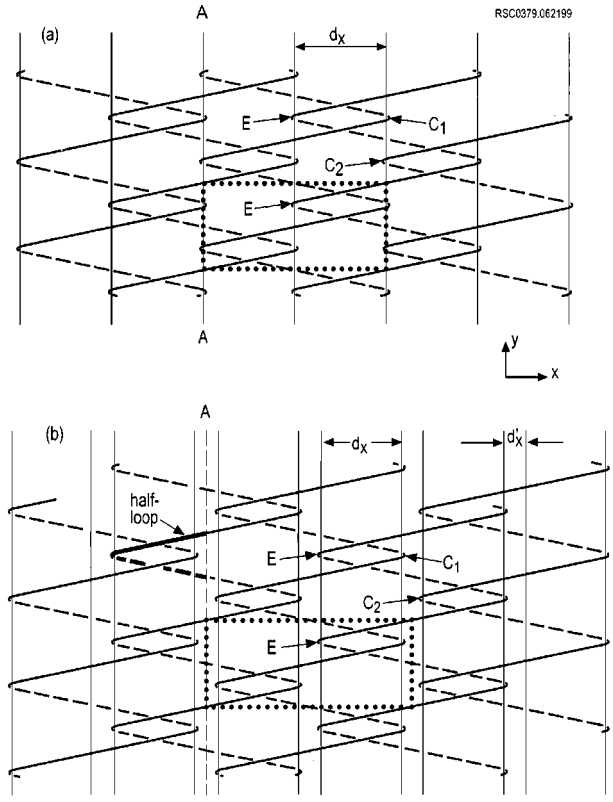

Figure 5 Two braid configurations. (a) Single pin system in which opposing crowns overlap above and below one another. (b) Dual pin system that can separate abutting crowns.

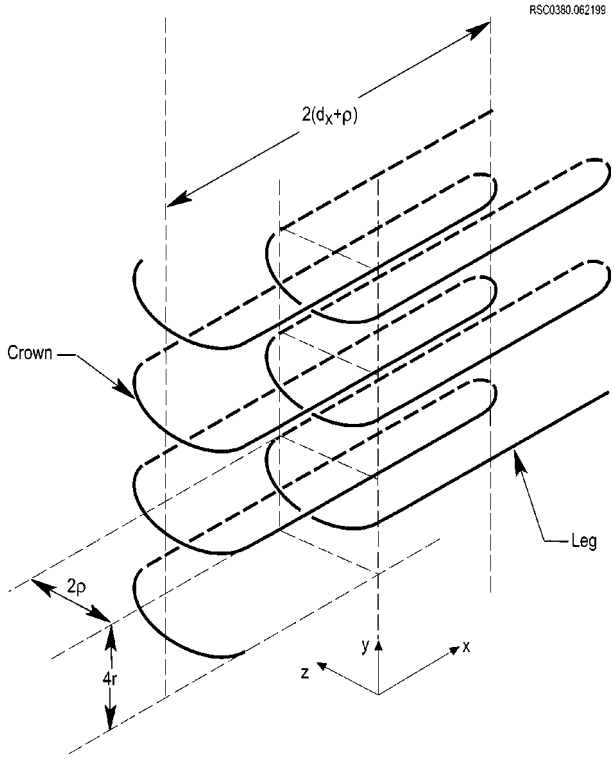

Figure 6 Schematic of two interpenetrating cords in a braided composite.

direction. The compacted fabric can therefore collapse into a configuration where the straight tow segments are horizontal (parallel to the x-axis). In case (a), crown C_1 must remain above crown C_2. The straight segments of the cords will therefore remain at some angle θ to the x-axis after beating up.

Fig. 6 shows the loci of two cords in the collapsed configuration in a perspective drawing. The lines correspond to the axes of the cords.

Simple analysis of the geometry of the composites and their mechanical behaviour can be made by idealising the braid geometry. Each cord is assumed to consist of a sequence of straight segments (legs) alternating with curved segments (crowns) where the cord passes around a pin, as suggested by Figs 5 and 6. The crowns follow helical paths with radius of curvature R and legs and crowns both have circular cross-sections with radius r. Predictions for the area and volume fractions of fibers for this idealisation are presented in Appendix A.

3. Properties of braided composites

3.1. Tests on single tows

Indicative strengths, $\sigma_{cd}^{(ult)}$, were determined for the cords by testing single tows of dry Kevlar fibers, each with a yield of approximately 554 mm/g (16.2 k denier). The tests were conducted by potting the ends of tow segments in resin blocks and loading in uniaxial tension by gripping the blocks. The tested gauge length was approximately 120 mm. Failure by fiber rupture generally occurred away from the blocks. The strength was recorded as the failure load divided by the total cross-sectional area of fibers in the tow, 1.24 mm^2.

The first series of tests determined the strengths of splice joints. The lap-joint splices eventually preferred for specimen fabrication showed values of $\sigma_{cd}^{(ult)}$ between 1.8 and 2.2 GPa. Even though failure usually occurred in or adjacent to the splice, the spliced tows were comparable in strength to pristine Kevlar fiber bundles of the same gauge length.

The second series of tests were conducted on looped specimens, which were formed by bending two tow segments into half loops and linking them together in the same way as two interpenetrating half loops would be linked in the composite (Fig. 5). Thus each end of the specimen comprised two tow ends, potted together in a resin block. The reported strengths from these tests were defined as the failure load divided by the cross-sectional area of the fibers in two tows, 2.48 mm^2. Values of $\sigma_{cd}^{(ult)}$ for these tests ranged from 550 to 700 MPa. Thus the strength of a cord can be expected to be reduced by a factor of about three by the stress concentration associated with loop intersection.

3.2. Specimens and tests

All specimens were fabricated in the pattern of case (a) (Fig. 5a) on a frame with uniformly spaced pins with $d_x = 12.7$ mm and with processing as described in Section 2. Other specimen details are summarised in Table II. Braiding was terminated after 4, 6, or 10 courses of loops had been formed, each course corresponding to two turns of a cord in the y direction of Figs 5 or 6. All specimens were approximately 200 mm long, with lateral dimensions, l_y and l_z, as tabulated. The lateral dimensions refer to a so-called core region, which contained all the fiber reinforcement but

TABLE II Composite specifications and properties

Specimen	BR5798a	BR5798b	BR5798c	BR6298a	BR6298b	BR6298c
Cord	S2	S2	S7	S1	S7	S7
Features[a]	Wrapped/ interlaced	Wrapped/ interlaced	Wrapped	Wrapped/ interlaced	Wrapped/ interlaced	wrapped/Al_2O_3 in matrix
Courses	4	4	8	10	4	4
l_y (mm)	26.7	29.7	28.7	15.2	28.4	30.0
l_z (mm)	13.7	15.0	18.5	9.7	12.2	11.1
A_{cd} (meas[d.])	0.078	0.064	0.147	0.127	0.151	0.156
V_f (meas[d.])	0.22	0.18	0.36	0.30	0.38	0.42
β	2.9	2.9	2.2	5.3	2.2	2.2
Failure[b]	del	del	del	loc	loc	del
Peak stress σ_p (MPa)	78	32	91	84	146	33
Strain at peak stress ε_p	0.4	0.25	0.4	0.07	0.08	0.02
Strain at ultimate ε_{ult}	1.4	2.0	1.0	0.3	0.8	1.3
W/volume W_v (MJ/m^3)	27.5	18	28.5	4.5	22	15
W/mass W_m (J/g)	17.5	11.5	18.5	3	14.5	10

[a]See text for details.
[b]"del" = delocalised; "loc" = localised.

excluded any peripheral zones of pure resin. Peripheral resin extends to the dimensions of the mold, whereas the reinforcement is compacted into a smaller volume. The peripheral resin cracks many times very early in the failure process and does not affect the composite behaviour.

The fiber volume fractions reported in Table I were calculated by measuring the total length of cords incorporated into the braids during braiding, multiplying by the cross-sectional area of fibers expected for a cord of the given yield, and dividing by the volume of the core region. The area fraction, A_{cd}, refers to the fraction of planes $A-A$ in Fig. 5a occupied by the legs of cords (including internal resin or void), calculated according to

$$A_{cd} = \frac{2n_{course}\pi r^2}{l_y l_z} = \frac{2n_{course}}{l_y l_z f\rho\psi} \qquad (2)$$

where n_{course} is the number of courses of loops.

The matrix in all specimens consisted of student-friendly Epofix resin[§], cured at 50°C for two hours. Various measures were sometimes built into the composite to resist matrix loss during loading to large strains. In all cases, additional Kevlar tows were wrapped by hand in helices around the outside of the fabric, working along an axis parallel to the x-direction. In some cases, additional Kevlar tows were interlaced in the y direction through the channel-like cavities of the braided loops. In one specimen, the resin was reinforced with chopped Al_2O_3 fibers approximately 10–20 mm long, stuffed by hand into the loop cavities.

Uniaxial tension tests were carried out in a screw-driven machine at low strain rates. All specimens were straight bars, as formed in the mold. To enhance gripping, steel pins were sometimes inserted into the ultimate loop cavities of the braid before resin infiltration, with their ends left protruding from the specimen. The pins were then inserted into slots in the grips. This eliminated slippage in the grips, which otherwise can be a difficult problem. Even at high grip pressures, disintegration of the specimen near the grips at high strains can cause loss of shear load transfer.

[§] Struers Co., Westlake, Ohio.

3.3. The achievement of delocalized failure

In four of the reported tests, completely delocalised failure was achieved. Fig. 7 shows the appearance of two such specimens after testing. The braided loops have been drawn out into intimate contact over the whole gauge length without reinforcement failure. (The less damaged regions at either end were in the grips.) The black shrink-wrap tubing has been torn in many places, but the fibers within the tubing have suffered minimal damage. In Fig. 7b, wrapping Kevlar yarns can still be seen in the less damaged regions. Ultimate failure ensues by rupture of the cords, not usually at splices.

The first damage observed in all specimens at relatively low strains consists of matrix cracking. The cracks are at first predominantly normal to the load axis, but develop into cracks of complicated shape with some segments parallel to the load axis at higher strains. When failure is delocalised, resin fragments are lost from the composite at strains exceeding approximately 0.1, but some resin remains out to much higher strains.

In the two specimens exhibiting localised failure, damage was confined to a limited region of the gauge section. In the case of specimen BR6298b, this band still extended over approximately one third of the gauge length and included substantial loop displacement and resin ejection. In this specimen, splice failure was observed well before ultimate failure, leading to the conjecture that the splice was unusually weak. Reasons for the localised failure in specimen BR6298a will be discussed below.

3.4. Stress-strain response and energy absorption

Records of engineering stress, σ_a, vs. engineering strain, ε_a, are presented in Fig. 8. Each record shows an initial phase of monotonically increasing stress,

(a)

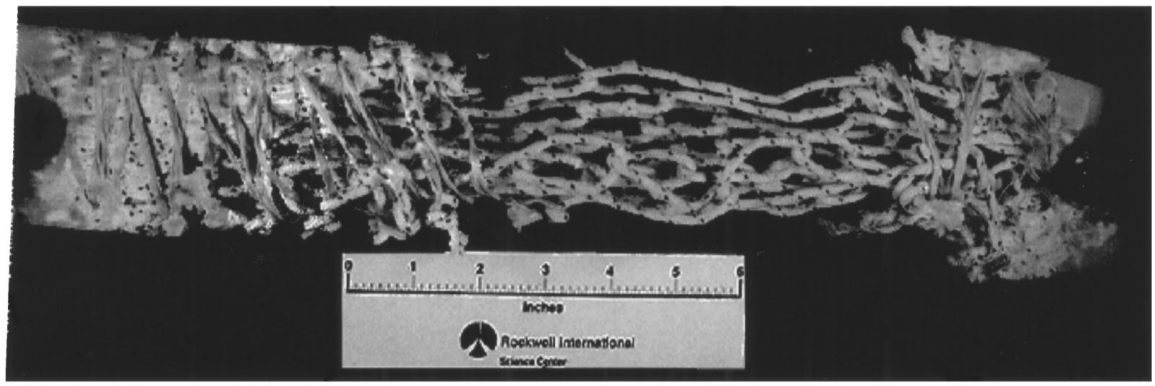

(b)

Figure 7 Failed composites showing lock up of loops following delocalized damage.

reaching a peak stress, σ_p, at some strain, ε_p. Values of σ_p range from 30 MPa to 140 MPa and values of ε_p from 0.1 to 0.4 (Table II). Stress variations following the peak vary from specimen to specimen. In one specimen that suffered localised failure (specimen BR6298a), the load plummeted almost to zero following the peak, although it remained nonzero out to moderately large strains during a phase of unraveling and pullout of ruptured cords. In other specimens, the stress dropped to levels in the range 20–40 MPa, remaining there to strains not far from the ultimate strain, ε_{ult}, listed in Table II. The region following the peak load is often punctuated by numerous drops and spikes in the load, corresponding to periods of resin fracture and ejection of resin fragments.

In all specimens, damage tends not to develop uniformly over the whole gauge section, even though, in cases of delocalised failure, the whole gauge section is uniformly damaged and strained prior to ultimate failure. Large strains usually develop in one region of the specimen, in a band involving two to three loops or, in other words, an interval of length approximately $2d_x$ (25 mm) along the x-axis. When the damage in the band is mature (loops in direct contact with one another or local strain $\varepsilon \approx \varepsilon_{ult}$), damage spreads to neighbouring material. Peak load usually corresponds to maturation of the damage in the initial band. In cases where the stress following the peak is considerably lower than the peak stress, one infers that the development of similar damage in neighboring material is facilitated by the pre-existing damage in the initial band. A mechanism for this effect will be suggested in the next section.

The energy absorbed per unit volume of the original gauge section, W_v, is given by the area under the engineering stress-strain curve[¶]:

$$W_v = \int \sigma_a \, d\varepsilon_a \tag{3}$$

When damage is delocalised, values range from 15 to nearly 30 MJ/m^3 (Table II). The specific energy

[¶] For Equations 3 and 4 to yield material constants, damage must be uniform over the gauge length and the stress to displace loops must be independent of location in the gauge length. This is not the case for all the specimens tested. Damage was nonuniform in the two specimens suffering localised failure and the stresses varied as the damage progressed through the others. However, the latter stress variations were relatively modest and therefore the figures quoted for energy absorption in the cases of delocalisation ought to be reasonably indicative of material properties.

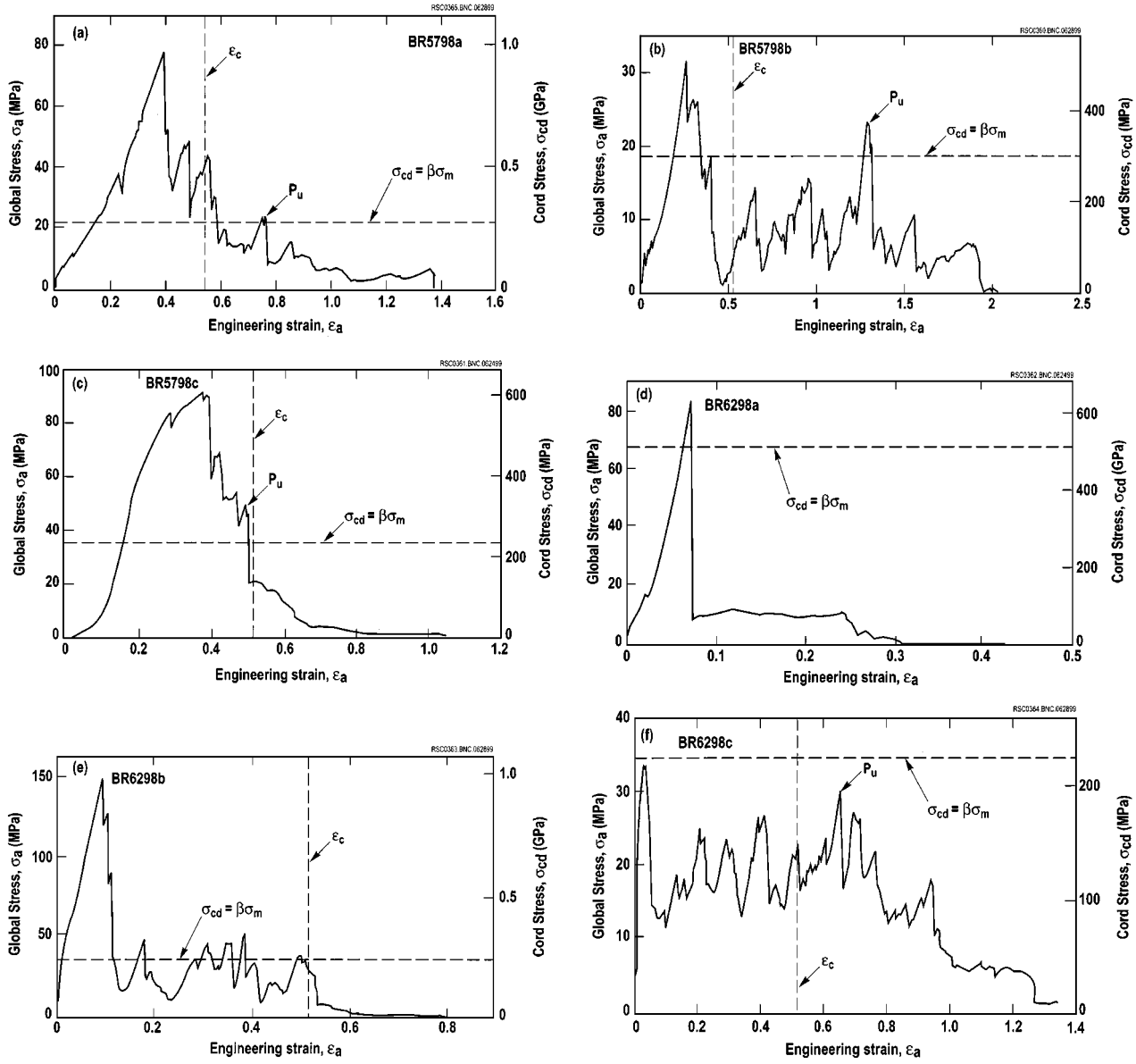

Figure 8 Engineering stress–engineering strain records for the specimens of Table I.

absorption, W_m, i.e., the energy absorbed per unit mass, is related to W_v by

$$W_m \frac{W_v}{\rho} \tag{4}$$

with ρ the composite density. Values of W_m range from 10 to 18 J/g.

4. Mechanisms

4.1. Prediction of the displacement stress

Some insight into the mechanics of delocalization and damage progression in the braided composites can be inferred from a model developed by Gong and Zok [2] for chain composites such as that depicted in Fig. 1. The model predicts the tensile stress component in the centers of the legs of the links (on the plane $A - A$ in Fig. 1) as the links are dragged through the matrix.

The matrix is modeled as a rigid/perfectly plastic medium. Stress transfer into the links from the matrix during the displacement can be partitioned into several contributions. 1) The resin trapped in near hydrostatic compression between two links as they approach one another exerts pressure over the inner surface of the crown of each link. 2) Shear tractions develop over the crown as it slides through the matrix. 3) Tensile tractions act on the outer surface of the crown where the matrix is being pulled apart between the crowns of abutting links, at least until the matrix fails along the line $A - A$. 4) Shear tractions act over the legs as the links slide through the matrix. The sum of the four contributions, when resolved in the direction of the motion of the links, must be balanced by tension in the legs, which takes its maximum value, $\sigma_{max}^{(leg)}$, at the centre of the legs. All four are proportional to the matrix shear flow stress, σ_m, the constants of proportionality depending on the link geometry.

The model is developed by considering the interaction of just two interpenetrating half-links. But this is exactly the geometry of two interpenetrating half-loops in a braided composite, at least in the geometrical idealization introduced in Section 2. Therefore, the problems of dragging two braided loops or two chain links

towards one another can be expected to have many similarities. The chain model is a good starting point for discussing the braided composites.

The results obtained in [2] can be summarised as follows, using the notation of this paper (note especially that R has different definitions in [2] and here). The stress in the centre of the leg of a braided loop is related to the matrix flow stress by

$$\sigma_{\max}^{(\text{leg})} = \beta\sigma_{\text{m}}$$
$$\beta \equiv \frac{2}{\pi}(C_1 + C_2 + 3.664C_3)\left(1 + \frac{R-r}{r}\right) - \left(\frac{C_1 - C_2}{2}\right) + C_4\frac{2d_x}{r} \quad (5)$$

where C_1, C_2, C_3, and C_4 are dimensionless constants of proportionality corresponding in order to the four contributions listed above. Equation 5 is restricted to links consisting of semi-toroidal crowns connected by cylindrical legs, which is the standard geometry of commercially available chains and a reasonable approximation for the braided loops. For unbonded, frictionless cord/matrix interfaces*, all load transfer from matrix to cord occurs on the compressive side of the crown and the proportionality factor β reduces to the even simpler result

$$\beta = 0.36 + 1.69\frac{R-r}{r} \quad (6)$$

Values are shown for β in Table II. They range approximately from 2 to 5. If the cord/matrix interfaces are strong, then much higher values result for β, ranging approximately from 10 to 20 for the cases of interest here (using results for C_1, etc., from [2]).

For either strong or weak interfaces, if the matrix is much more compliant than the reinforcement, as is epoxy resin relative to Kevlar, then Equation 5 multiplied by the area fraction, A_{cd}, should be approximately equal to the composite stress during link displacement. This is shown in Fig. 8 by the line marked "$\sigma_{\text{cd}} = \beta\sigma_{\text{m}}$", where σ_{cd} is the value of $\sigma_{\max}^{(\text{leg})}$ predicted by Equation 5 in the limit of Equation 6 (weak cord/matrix interfaces – lowest values of β).

Also marked in Fig. 8 is the expected strain to lockup, ε_{c}, which is (Appendix A)

$$\varepsilon_{\text{c}} = \frac{1}{2} + \frac{R-r}{d_x}. \quad (7)$$

Loop displacement through the matrix might be expected to occur mainly at strains below ε_{c}.

* The interfaces in question are not those between individual fibers and resin. Fiber/resin interfaces are usually relatively strong and do not commonly fail during composite failure. The relevant interfaces are instead those between entire cords and the surrounding matrix. When these debond, they do so by means of a peripheral matrix crack that separates the cord as an entity from its environment.

4.2. Mechanisms underlying the stress-strain curves

Consider first the three specimens other than the specimens that suffered localised failure and the specimen whose matrix was strengthened with chopped Al_2O_3 fibres, i.e., the specimens of Fig. 8a–c. For these specimens, the strain to peak stress, ε_{p}, is quite high–in the range 0.1 to 0.4. The peak stress therefore occurs when substantial damage has already pervaded the specimen. The damage must include significant link displacement, at least in the initial damage band. Yet the peak stress far exceeds the stress for loop displacement, $\beta\sigma_{\text{m}}$ (Fig. 8a–c). This implies that, in spite of the extensive damage to the matrix at peak stress, there is still sufficient coupling between the cords and the matrix that the constraint factor, β, has a value somewhat larger than its value for weak (debonded) cord/matrix interfaces. Observations were not sufficiently detailed to confirm this conjecture (details are difficult to see in the midst of widespread damage), but one would expect that the additional load transfer to the legs probably comes through strong friction around the legs, which is assumed zero in Equation 6.

Since premature cord rupture or splice failure was not observed in these cases, the load drop following peak stress in Fig. 8a–c is probably associated with loss of matrix material and loss of frictional contact with the legs of the displacing cords. Since the difference in values of β for debonded, stress-free interfaces and interfaces with some load transfer is quite pronounced, the fall in stress can be large.

In the case of the specimen with Al_2O_3 reinforced fibres (Fig. 8f), the strain to peak stress is relatively small ($\varepsilon_{\text{p}} = 0.02$) and the peak stress is very near the predicted displacement stress for weak interfaces. One can speculate that the Al_2O_3 fibres have embrittled the matrix, so that it could not follow the displacements of the cords and broke away from them much earlier.

For the four cases of delocalised failure, the stress in the period following the peak stress and up to or somewhat beyond the expected lockup strain, ε_{c}, is not far from the prediction of σ_{cd} for weak interfaces. Here the chain link model seems to work quite well. With corroborating observations from tests, the validity of the description of the mechanics of link displacement embodied in Equation 5 is confirmed.

In the two specimens fabricated with cords contained in shrink-wrap tubing, relatively large stresses were sustained well beyond the nominal lockup strain, ε_{c} (Fig. 8a and b). The shrink wrap tubing creates a fairly stiff cord that does not turn around the dowel pins during braiding as easily as the served cords. Consequently, the shrink-wrapped cords tend to bow out more in the braided fabric, with crowns of larger radius of curvature and shorter legs (Appendix A). Under the high loads of a test, the loops can stretch by changing their shape, raising the effective strain to lockup. This effect could account for test strains approaching 1. Even higher recorded strains correspond to the last gasps of a specimen's strength after one or more cords has ruptured and is unraveling through the fabric. This process can sustain appreciable stress levels and also accounts

for the tail of the curve ($\varepsilon_a > 0.6$) for the specimen with Al_2O_3 reinforced matrix (Fig. 8f). The presence of the Al_2O_3 fibers inhibits unravelling.

In all the specimens exhibiting delocalised failure, a minor peak can be identified at about the lockup strain (or somewhat beyond it for the shrink-wrap tubing specimens) beyond which the stress declines fairly steeply and monotonically to zero. These points have been labeled P_u. While direct observations were inconclusive (because of the high level of damage accrued prior to such strains), this peak can be conjectured to correspond to the failure of a cord. The stress in the cords at P_u (right hand ordinate of Fig. 8) ranges from 200 to 350 MPa (Fig. 8a–c and f), which corresponds, for a fiber packing factor of 0.7, to fiber stresses ranging from 340 to 500 MPa. This is somewhat lower than $\sigma_{cd}^{(ult)}$ determined from loop tests (550–700 MPa), suggesting that the cords are weakened by the damage sustained during loop displacement.

The localised failure observed in the specimen fabricated with thin cords (Fig. 8d) is now easily understood. For a thin cord, the ratio $(R - r)/r$ is large, the factor β is therefore large, and the stress required to displace loops ($\sigma_{cd} = 550$ MPa) is larger than the cord strength.

In several cases, the stress for loop displacement following peak stress is markedly lower than the predicted displacement stress (Fig. 8b and f). This probably signifies loss of matrix material that was previously trapped between two loops, which will lower the effective constraint factor, β. A similar effect occurs in chain/epoxy composites [3]. In braided composites, it can be exacerbated by separation of the legs of loops in the y-direction, which can be wedged apart by the entrapped matrix as they are drawn towards one another. This can happen relatively easily in the braided composites, because the legs are highly anisotropic unidirectional composites that are strong in tension but weak in axial shear; and the braided loops are not closed like chain links.

Loop displacement prior to peak stress commonly (but not always) occurs at significantly higher stresses than loop displacement following peak stress. This and the fact that damage prior to the peak stress occurs mainly in the initial damage band implies that preexisting damage to large strains in adjacent loops facilitates loop displacement. It is possible that loop spreading in the previously damaged material promotes matrix cracking in neighbouring regions, facilitating matrix loss and the reduction of the constraint factor, β.

5. Potential for energy absorption

The values of energy absorption for the braided composites are very encouraging, but substantially higher values could be obtained by better design and processing. The energy absorption will be maximized by 1) raising the fiber volume fraction; 2) using the strongest possible reinforcing fibers; 3) choosing a matrix with a flow stress, σ_m, for which the product $\beta\sigma_m$ is as great as possible without exceeding the reinforcement strength, $\sigma_{cd}^{(ult)}$; and 4) preventing the premature loss of matrix from between loops by brittle matrix fracture and fragment ejection.

The fiber volume fraction, V_f, can be raised in several ways. Fabricating composites in which crowns abut without overlapping, such as in Case (b) of Fig. 5, will immediately raise V_f by up to 50%. Benefit will also come from starting with a supply of fiber cords, such as fibers wrapped in wound yarns, that have been prepared in an automated serving apparatus to high consistency and therefore higher fiber packing factors. Further developments of compacting apparatus will also enable a tighter fabric arrangement in the mold.

The effective fiber strength can be improved by minimising fiber damage during loop displacement, which currently degrades cord strength by approximately 40%. A more effective protective sheath than the shrink wrap tubing could be developed; and matrices such as elastomers that are more ductile than the epoxy resin might be less abrasive.

In this work, reinforcing the matrix with Al_2O_3 fibers was tried as a method of resisting matrix loss during loop displacement. An alternative route that may work better would be to use an elastomeric matrix, such as natural rubber.

With such modifications, goals of 100 MJ/m^3 for the energy absorbed per unit volume and 50 J/g for the specific energy absorption would seem to be attainable.

6. Scale changes

As far as the model of loop displacement embodied in Equation 5 is correct, the stress required for loop displacement will be unchanged by changes in the scale of the reinforcement that maintain similarity. The displacement stress depends only on the ratios R/r and d_x/r, not on their absolute values. Likewise, the area fraction, A_{cd}, depends only on ratios of lengths (Equations A.4 and A.9) and so the global stress required for cord rupture will be invariant under changes in scale (apart from possible size effects in the statistics of fiber bundle strength). Thus there may be neither advantage nor disadvantage for energy absorption in producing finer or coarser braids.

If the cords can decouple relatively easily from the matrix, as in all the composites reported here, then the stress for loop displacement will also be neutral with respect to changes in the loop aspect ratio, d_x/r. If, however, the cords can remain coupled to the matrix through large displacements, then the stress in the legs of the cord can rise quite dramatically with d_x/r. The constraint factor, β, is much higher when load transfer along the legs is significant [2]. Where this occurs, the efficacy of the matrix in resisting loop displacement, and therefore in taking best advantage of the strength of the cords, is enhanced. Furthermore, the surface area of the legs varies as $d_x r$ while A_{cd} varies as r^2, so the matrix resistance will rise if the aspect ratio rises under conditions where the matrix and legs remain mechanically coupled.

Reduction of the scale of the reinforcement will be very important in reducing the sensitivity of the composite to intrinsic flaws, including unusually weak splices, or damage from an external source. The specimens tested here contained only a few loops across their width and were therefore especially vulnerable to a

weak flaw. If hundreds of courses of loops were present in the same volume, which would seem a reasonable achievement for an automated braiding process, then one poor splice would have little effect.

7. Summary remarks

A new class of braided composites has been presented that exhibit lockup mechanisms following loop displacement, thus delocalising damage and achieving high levels of energy absorption. The energy absorbed per unit mass is especially attractive.

The mechanisms of the progression to failure appear to be similar in many regards to those observed previously in chain composites. In particular, the stress required for loop displacement can be predicted to a useful approximation by a model developed for the chain composites. This allows some simple inferences about design optimization.

Further prospects for optimization lie in improving the volume fraction of reinforcing fibers, towards which automating the braiding process should be a major step, and selecting a tougher matrix to avoid premature loss of matrix during damage to large strains.

Appendix A. Model of the composite geometry

A simple model of the geometry of the braided loops aids material design and the analysis of stress distributions and mechanisms. The model shown here begins with the assumptions stated in Section 2.4, that the braided cords comprise straight legs and helical crowns with circular cross-sections of radius r. Their positions can be represented by the loci of their axes. The junctions of leg and crown segments are assumed to lie exactly at the x-coordinate of the centre of the pin around which the crown bends. The axis of the helical crown segment passes around a cylindrical surface of radius R. Thus $R = r_{\text{pin}} + r$, where r_{pin} is the radius of one of the pins.

Case (b) of Fig. 5, which has a slightly simpler geometry because of the avoidance of overlap of abutting crowns, will be dealt with first.

Case (b): Let d_x and d'_x denote the centre-to-centre separations of the pins, as indicated in Fig. 5b. Following compaction in the y direction, the legs in case (b) are horizontal. Since the cords rest directly on one another, the apexes of successive crowns such as those marked E in Fig. 5b must be separated by $4r$ (the diameter, $2r$, of one leg plus twice the half-thickness, r, of the crowns.) Therefore, the helix followed by each crown must have pitch $4r$ in one complete turn. The length of the axis of one representative half loop, s_1, such as that highlighted by bold lines in Fig. 5b, is the arc length of the helix over a half-turn plus the length of one leg, i.e.,

$$s_1 = \pi R\sqrt{1 + \left(\frac{2}{\pi}\frac{r}{R}\right)^2} + 2d_x + d'_x. \qquad \text{(A.1)}$$

The are four such half-loops in one unit cell. The dimensions of the unit cell are $2(d_x + d'_x)$, $4r$, and $2(R + r)$ in the x, y, and z directions, respectively, where the z-axis points into the page of Fig. 5 (see additional note below). Since the cross-sectional area of a cord is πr^2, the fraction of the composite occupied by the cords, V_{cd}, follows as

$$V_{\text{cd}} = \frac{\pi\left[\pi \bar{R}\sqrt{1 + (2/\pi R)^2} + 2\bar{d_x} + \bar{d'_x}\right]}{4(\bar{d_x} + \bar{d'_x})(\bar{R} + 1)} \quad \text{(case (b))} \qquad \text{(A.2a)}$$

where

$$\bar{R} \equiv \frac{R}{r} \quad \bar{d_x} \equiv \frac{d_x}{r} \quad \bar{d'_x} \equiv \frac{d'_x}{r}. \qquad \text{(A.2b)}$$

If the packing factor of the axial fibers in the cords is f, then the volume fraction of the axial fibers in the composite, V_{f}, is given by

$$V_{\text{f}} = f V_{\text{cd}}. \qquad \text{(A.3)}$$

A useful parameter for analyzing stress distributions is the area fraction, A_{cd}, of a plane such as that marked $A - A$ in Fig. 5a or b occupied by the legs of the cords. Since there are two legs crossing such a plane in each unit cell,

$$A_{\text{cd}} = \frac{\pi}{4}\frac{1}{\bar{R} + 1} \quad \text{(case (b))}. \qquad \text{(A.4)}$$

The strain capacity, ε_{c}, which is the engineering strain expected before interpenetrating loops come into direct contact with one another, is

$$\varepsilon_{\text{c}} = \frac{\bar{d_x} + 2[\bar{R} - 1]}{2[d_x + d'_x]} \quad \text{(case (b))}. \qquad \text{(A.5)}$$

Case (a): In case (a), the legs do not compact to loci parallel to the x-axis, but remain inclined to it at an angle θ. The right end of each leg segment sits higher than the left by the thickness, $2r$, of one crown (Fig. 5a), so that

$$\theta = \tan^{-1}\left[\frac{2r}{d_x}\right] \quad \text{(case (a))}. \qquad \text{(A.6)}$$

Inclination of the legs to the x-axis is visible in the specimen shown in Fig. 4. The pitch of the helical crowns is the same as in case (b), so the path length of a half-loop becomes

$$s_1 = \pi R\sqrt{1 + \left(\frac{2}{\pi}\frac{r}{R}\right)^2} + 2\sqrt{d_x^2 + (2r)^2} \quad \text{(case (a))}. \qquad \text{(A.7)}$$

The dimensions of the unit cell of Fig. (5a) are $2d_x$, $6r$, and $2(R + r)$ in the x, y, and z directions, respectively. The volume fraction occupied by the cords is thus

$$V_{\text{cd}} = \frac{\pi\left[\pi \bar{R}\sqrt{1 + (2/\pi R)^2} + 2\sqrt{\bar{d}_x^2 + 4}\right]}{6\bar{d_x}(\bar{R} + 1)} \quad \text{(case (a))}. \qquad \text{(A.8)}$$

The area fraction of the plane marked $A-A$ in Fig. 5a occupied by the legs is

$$A_{cd} = \frac{\pi}{6}\frac{1}{\bar{R}+1} \qquad \text{(case (a))}. \quad \text{(A.9)}$$

The strain capacity is given by

$$\varepsilon_c = \frac{1}{2} + \frac{\bar{R}-1}{d_x} \qquad \text{(case (a))}. \quad \text{(A.10)}$$

In both cases (a) and (b), the following restriction must hold for cords of circular cross-section:

$$\bar{d_x} \geq 2(\bar{R}+1). \quad \text{(A.11)}$$

In practice, the lower bound $\bar{R} \geq 2$ also holds, equality corresponding to a pin of radius equal to r.

The results for V_{cd} for cases (a) and (b) are plotted in Fig. A.1 for representative values of parameters. The fiber volume fraction, V_f, will typically be approximately 70% of V_{cd}. Some improvement over the estimates shown in Fig. A.1 can be achieved by compacting the composite, which reduces the gaps between legs in the y direction and achieves closer packing of both legs and crowns by squashing them into square rather than circular cross-sections.

Fig. A.2 shows a cross-sectional view of two interlacing half-loops in a compacted braid projected onto an $x-z$ plane. A similar figure appears in an appendix of [3] for two links in a steel chain composite. Inspection of Fig. A.2 reveals that, if the legs are assumed to sit directly on one another as shown (and as assumed in calculating the volume of the unit cells in Fig. 5) and the crowns remain toroidal, then the crowns of the two half-loops must interpenetrate. In dealing with steel chain links, this must be taken into account and the legs must remain separated. The fibrous cords, in contrast, can deform fairly easily under lateral loads. Thus they will reshape themselves as suggested in Fig. A.2 and the legs will come into contact. Indeed, since the legs can also change fairly easily from a circular cross-section, they can be pressed even closer together in practice than indicated by a centre-to-centre separation of $2r$.

Table A.I shows various parameters as predicted by the model and measured in specimens. For predictions of V_f, a packing factor $f = 0.7$ was assumed. The predictions and measurements agree quite well generally, with some significant variances. The dimension, l_z, is underestimated in several cases, especially for those specimens made with cords contained in shrink-wrap (BR5798a and BR5798b). This implies that the cords are too stiff to follow the radius of the dowel pins during braiding. For specimens made with served Kevlar tows where l_z is underpredicted (BR5798c and BR6298a), the probable cause is compaction in the x-direction in the mold, which causes bulging in the z-direction. Note that l_y is overpredicted for these two composites, whereas it is predicted correctly for the composites with shrink-wrapped cords.

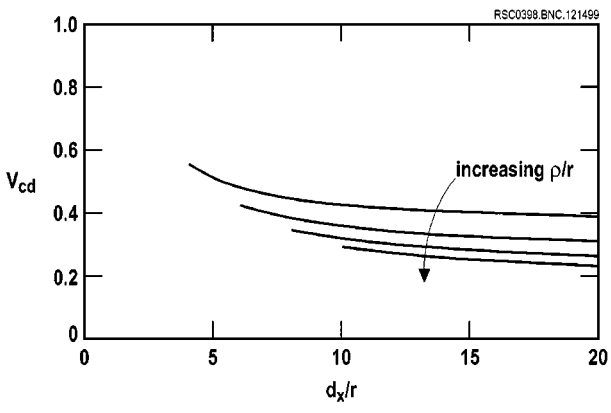

Figure A.1 The volume fraction of the composite occupied by cords in case (a) of Fig. 5.

TABLE A.I Measured and predicted dimensions and fiber volume fractions

	l_y expt (mm)	l_y model (mm)	l_z expt (mm)	l_z model (mm)	V_f expt	V_f model
BR5798a	26.7	25.5	13.7	9.6	0.22	0.28
BR5798b	29.7	25.5	15.0	9.6	0.18	0.28
BR5798c	28.7	51.8	18.5	11.8	0.36	0.34
BR6298a	15.2	32.7	9.7	6.5	0.30	0.19
BR6298b	28.4	34.6	12.2	11.8	0.38	0.34
BR6298c	30.0	34.6	11.2	11.8	0.42	0.34

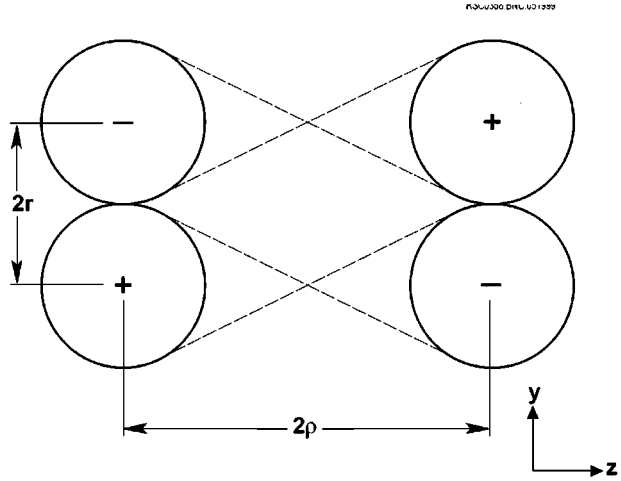

Figure A.2 Schematic of the cross-sections of two half-loops compacted in the y-direction. The plus and minus symbols indicate the direction in which the legs progress in or out of the page towards their crowns.

Acknowledgements

Work supported by the U.S. Army Research Office, Contract No. DAAH04-95-C-0050. The authors are very pleased to record the enthusiastic, patient, and skilful handicraft of Noemi Altamirano, Christian Berg, Jenny Garredo, Rachel Goldberg, Gloria Rios, Annalise Keen, and Amber Sands in supplying the numerous specimens consumed in this study. Helpful discussions with Drs. Sridhar Narayanaswamy and Frank Zok are also acknowledged.

References

1. B. N. COX, *J. Mater. Sci.* **30** (1996) 4871.
2. X. GONG, F. ZOK, B. N. COX and J. DAVIS, *Acta Materialia*, in press.
3. B. N. COX, J. DAVIS, N. SRIDHAR, F. ZOK and X. GONG, *ibid.*, in press.
4. B. N. COX and J. B. DAVIS, *Composites*, submitted.

Received 1 September 1999
and accepted 14 January 2000